Electronic Supplementary Information (ESI)

Seaweed-like phosphates/MOF heterostructure as a synergistic electrocatalyst for alcohol oxidation

Ya-Ya Sun,[a,c] Jia-Yang Luo,[a,c] Xue-Qian Wu,*[b,c] Ya-Pan Wu,[a,c] Shuang Li,[a,c] Ya-Meng Yin,[a,c] Hui-Juan Ma,[c] Ruan Chi [c] and Dong-Sheng Li *

[a] *College of Materials and Chemical Engineering, Key Laboratory of Inorganic Nonmetallic Crystalline and Energy Conversion Materials, China Three Gorges University, Yichang 443002, P. R. China.*

[b] *College of Electrical Engineering & New Energy, China Three Gorges University, Yichang 443002, P. R. China.*

[c] *Hubei Three Gorges Laboratory, Yichang 443007, P. R. China.*

Experimental section

1.1 Materials and characterizations

All the chemicals were commercially available and applied directly without any further purification. Powder X-ray diffraction (PXRD) was performed on a Rigaku Ultima IV diffractometer (CuKα radiation, λ = 1.5406 Å). FT-IR spectra were recorded on a Thermo Electron NEXUS 670 spectrometer as KBr pellets from 4000 to 400 cm^{-1}. An ESCA LABMKLL X-ray photoelectron spectrometer with an Al Kα source was employed to conduct X-ray photoelectron spectrometry (XPS) measurements. Scanning electron microscopy (SEM) and high-resolution transmission electron microscopy (HRTEM) images were taken using a JSM-7500F and JEOL JEM 2010F at an accelerating voltage of 200 kV, respectively. Thermogravimetric (TG) curves were obtained on a TGA-50 thermogravimetric analyzer with a heating rate of 10 ^oC min^{-1} under air atmosphere. A LabRAM Aramis Raman spectrometer was used to record Raman spectra.

1.2. Materials preparation

1.2.1 Preparation of MOF-74

Original MOF-74 was synthesized according to the previously reported literature.[1] 2,5-dihydroxyterephthalic acid (H_2DOBDC, 1.2 mmol, 95.8 mg) and $Ni(NO_3)_2{\cdot}6H_2O$ (1.0 mmol, 290.8 mg) were dissolved in 30 mL dimethylformamide/ethanol/H_2O (DMF/EtOH/H_2O, 1/1/1, V/V) mixed solvents in a 50 mL Teflon-lined stainless steel vessel. The mixture was transferred to an oven and heated at 120 ^oC for 48 h. After cooling to room temperature, yellow microcrystalline sample can be obtained after washing several times with ethanol and filtration.

1.2.2 Preparation of $Co_3(PO_4)_2$

A mixture of $CoCl_2{\cdot}6H_2O$ (1.0 mmol, 237.9 mg), NaH_2PO_4 (2.3 mmol, 320 mg), 3 mL DMF and 5 mL H_2O was added into a 20 mL Teflon-lined stainless steel vessel after stirring for 1 h, heated at 160 ^oC for 16 h, and then cooled to room temperature. The resultant purple powder product can be harvested by centrifugation and washed three times with deionized water.

1.2.3 Preparation of $Ni_3(PO_4)_2$

The preparation procedure for $Ni_3(PO_4)_2$ was similar to that of $Co_3(PO_4)_2$ by using $NiCl_2{\cdot}6H_2O$ (1.0 mmol, 237.6 mg) in the place of $CoCl_2{\cdot}6H_2O$.

1.2.4 Preparation of $Co_3(PO_4)_2/Ni_3(PO_4)_2$/MOF-74-*x* heterostructures

50 mg MOF-74 powder and 50 mg $Co_3(PO_4)_2$ sample were added into a mixed solvent of DMF/H_2O (5 mL/5 mL) under stirring for 2 h. Subsequently, the above mixture was transferred into a 20 mL Teflon-lined stainless steel vessel, and heated at 160 ^oC for 16 h. The $Co_3(PO_4)_2/Ni_3(PO_4)_2$/MOF-74-1 composite (gray powder) was obtained after cooling to room temperature, washed three times with ethanol, and dried under vacuum condition. Other heterogeneous composites were prepared similarly by adjusting the reactant ration of MOF-74/$Co_3(PO_4)_2$ from 2:1 to 4:1.

1.2.5 Electrochemical measurements

All the electrochemical measurements were carried out in a traditional three-electrode system at room temperature by using CHI660e electrochemical workstation. A modified glassy carbon electrode (GCE, 3 mm inner diameter, 0.0706 cm^2), a Hg/HgO electrode, and a Pt wire were applied as working, reference and counter electrodes, respectively. The catalyst ink was prepared by dispersing the sample (4 mg) into a mixed solution (3 mL) containing EtOH (2 mL), deionized water (0.8 mL), and a 5 wt% Nafion solution (0.2 mL), followed by ultrasonication for 1 h. The catalyst suspension (4 μL) was dripped on the surface of GCE (normalized to the loading area with 0.38 mg cm^{-2}), and then the working electrode was air-dried and kept in a desiccator. The static cyclic voltammetry (CV) measurement was typically performed in N_2-saturated 0.1 M KOH solution, and the electrocatalytic performance of the materials toward MOR/EOR was evaluated in N_2-saturated 0.1 M KOH + 1.0 M CH_3OH (EOR: 0.1 M KOH + 1.0 M CH_3CH_2OH) electrolyte with different scan rates. The working electrode was electrochemically activated with a certain cycling window until the CV curves tended to coincide before electrochemical tests.

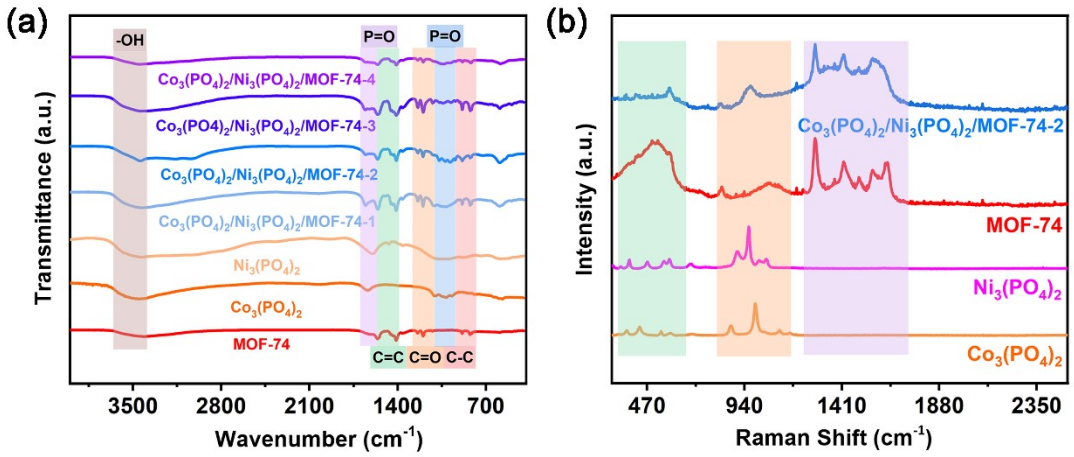

Fig. S1. (a) FT-IR spectra and (b) Raman spectra of MOF-74, $Co_3(PO_4)_2$, $Ni_3(PO_4)_2$, and as-obtained $Co_3(PO_4)_2/Ni_3(PO_4)_2$/MOF-74-*x* heterogeneous composites with different ratios.

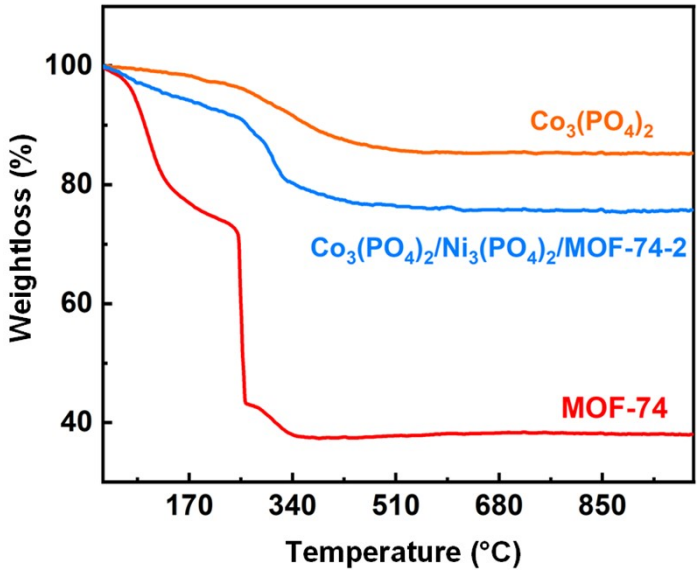

Fig. S2. TGA curves of MOF-74, $Co_3(PO_4)_2$, and as-obtained $Co_3(PO_4)_2/Ni_3(PO_4)_2$/MOF-74-2 composite.

As shown in Fig. S2, MOF-74 shows two main steps of mass loss (62.5%), corresponding to the release of guest solvent molecules and the decomposition of the overall framework. $Co_3(PO_4)_2$ exhibits a single step of weight loss of 14.3% from 90 to 560 °C. As predicted, the TGA curve of $Co_3(PO_4)_2/Ni_3(PO_4)_2$/MOF-74-2 includes the pyrolysis processes of the three individual components with a total loss of 24.3%. The ICP-MS revealed that the representative heterojunction contains 9.6 wt% Ni and 28.6 wt% Co.

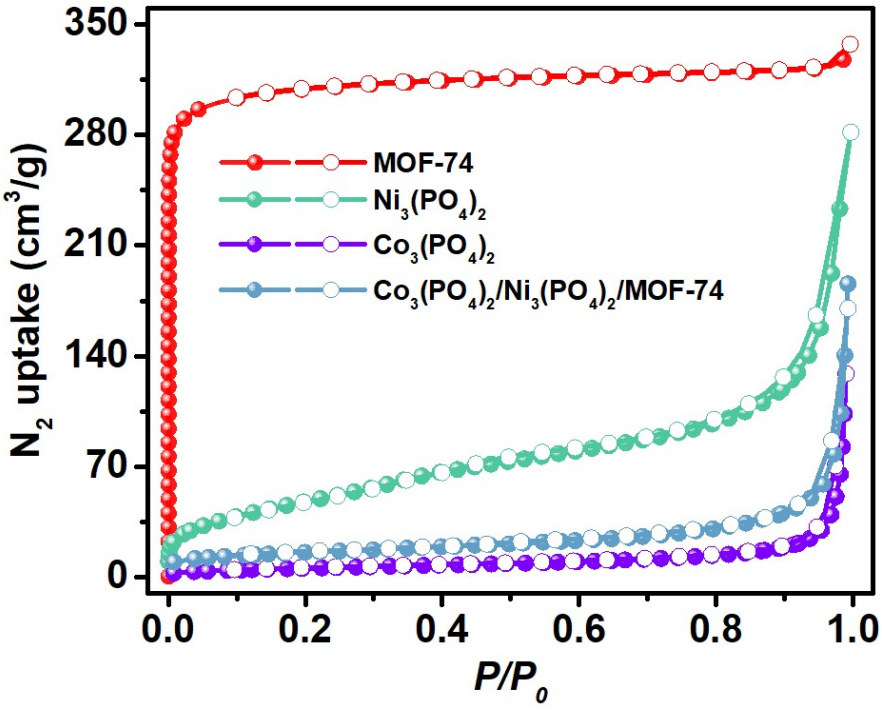

Fig. S3. N_2 adsorption/desorption isotherms of the $Co_3(PO_4)_2$, $Ni_3(PO_4)_2$, MOF-74 and $Co_3(PO_4)_2/Ni_3(PO_4)_2$/MOF-74-2 samples at 77 K.

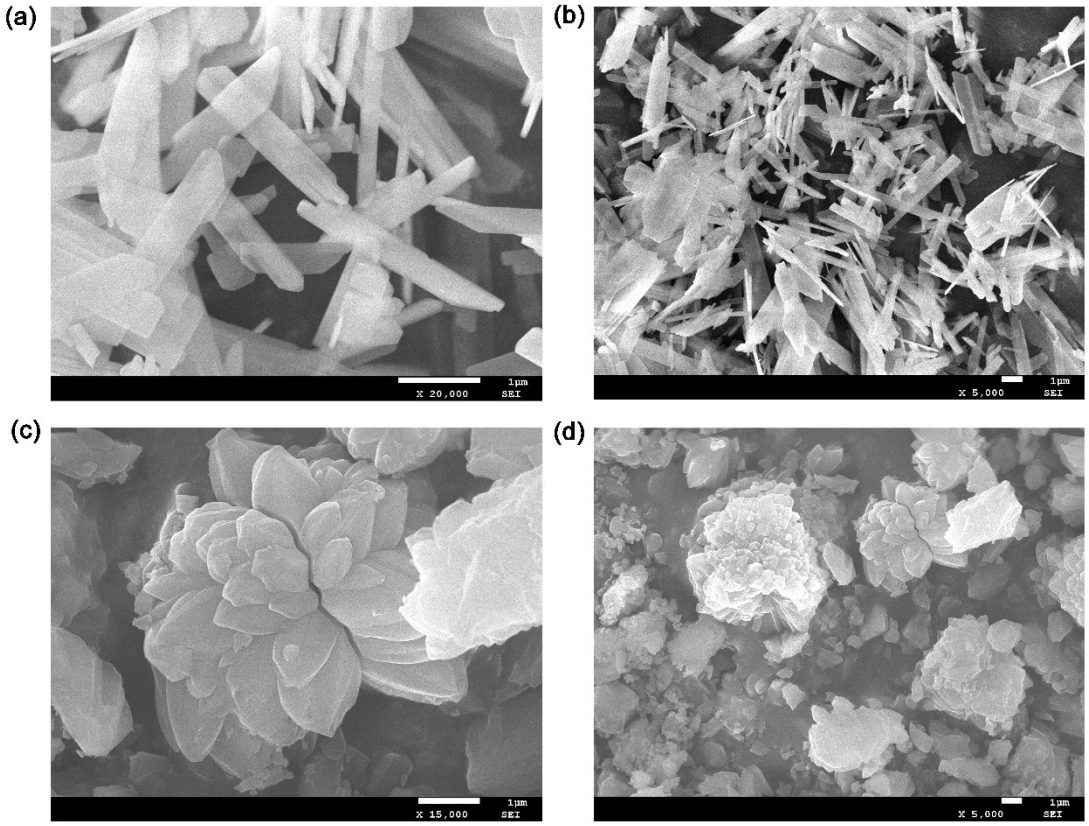

Fig. S4. (a), (b) SEM images of the $Co_3(PO_4)_2$ and (c)/(d) MOF-74 samples.

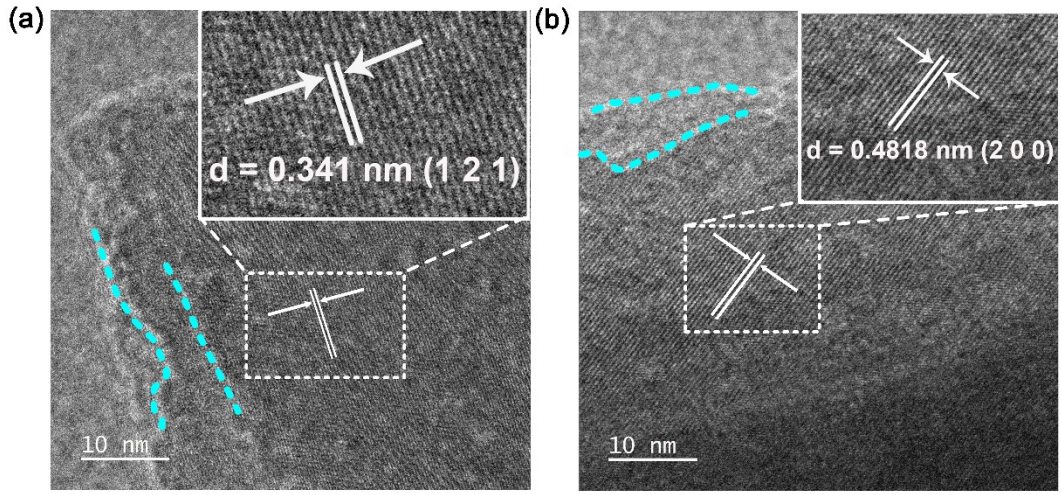

Fig. S5. TEM images of $Co_3(PO_4)_2/Ni_3(PO_4)_2$/MOF-74-2 heterojunction.

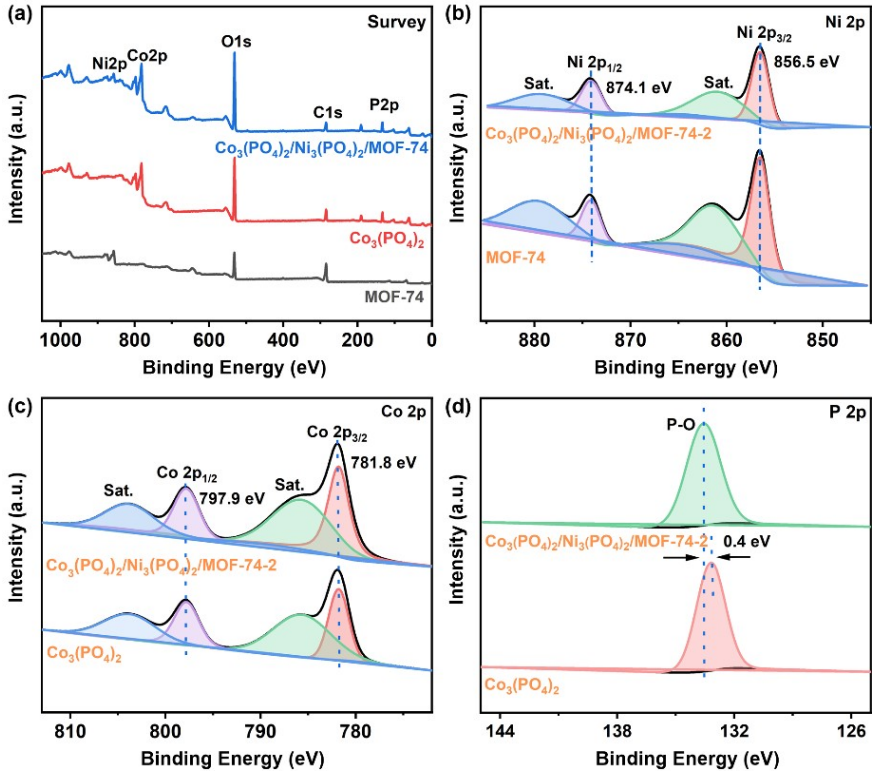

Fig. S6. (a) XPS survey of MOF-74, $Co_3(PO_4)_2$ and $Co_3(PO_4)_2/Ni_3(PO_4)_2$/MOF-74-2; (b) Ni 2p, Co 2p and P 2p spectra for MOF-74, $Co_3(PO_4)_2$ and $Co_3(PO_4)_2/Ni_3(PO_4)_2$/MOF-74-2.

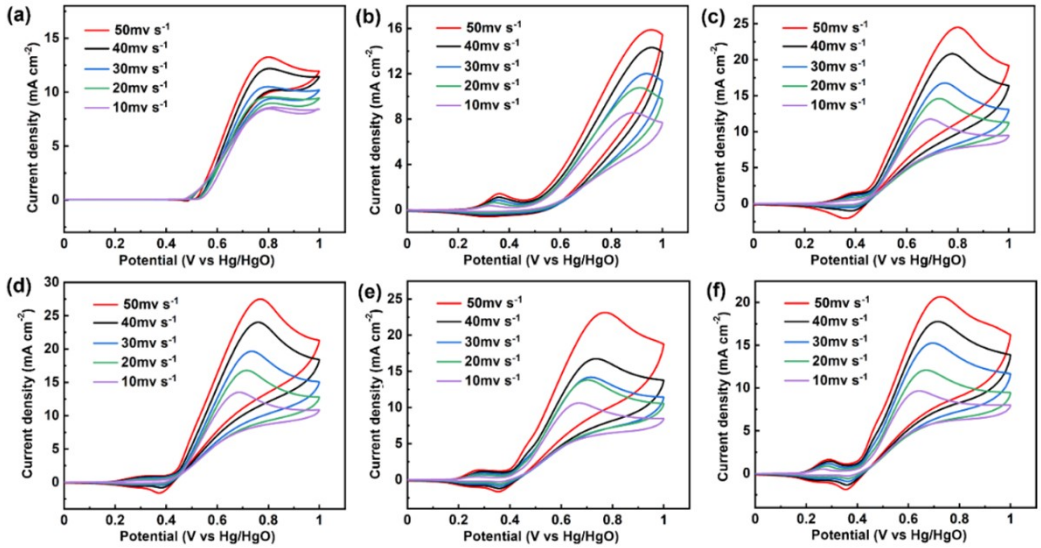

Fig. S7. CV curves of (a) MOF-74, (b) $Co_3(PO_4)_2$, and (c) $Co_3(PO_4)_2/Ni_3(PO_4)_2$/MOF-74-*x* (*x* = 1, 2, 3, 4) heterojunctions.

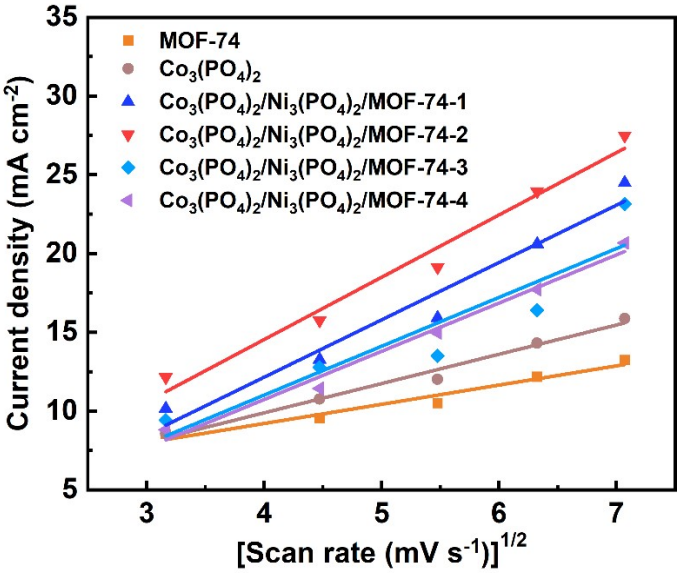

Fig. S8. The linear relationship between current densities and the square root of scan rates in 0.1 M KOH + 1.0 M CH_3OH for MOF-74, $Co_3(PO_4)_2$, and $Co_3(PO_4)_2/Ni_3(PO_4)_2$/MOF-74-*x* (*x* = 1, 2, 3, 4) heterojunctions.

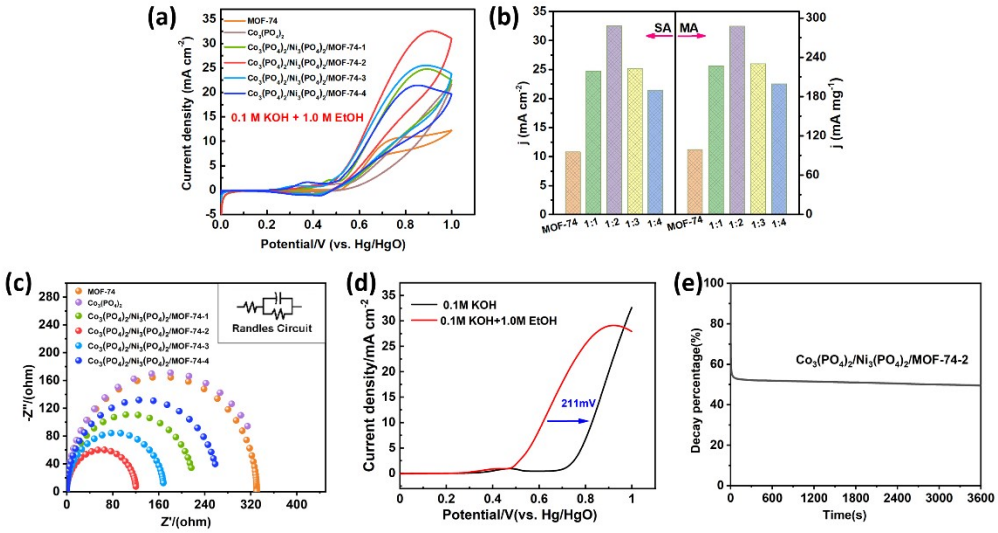

Fig. S9. (a) CV curves for EOR of different catalysts in 0.1 M KOH with 1.0 M CH_3CH_2OH; (b) Bar chart of mass activities (MA) and specific activities (SA) of as-obtained catalysts for the EOR; (c) Nyquist curves of EIS for different catalysts; (d) LSV curves of $Co_3(PO_4)_2/Ni_3(PO_4)_2$/MOF-74-2 in 0.1 M KOH solution or with 1.0 M CH_3CH_2OH; (e) Chronoamperometric curve of $Co_3(PO_4)_2/Ni_3(PO_4)_2$/MOF-74-2 in 0.1 M KOH + 1.0 M CH_3CH_2OH solution.

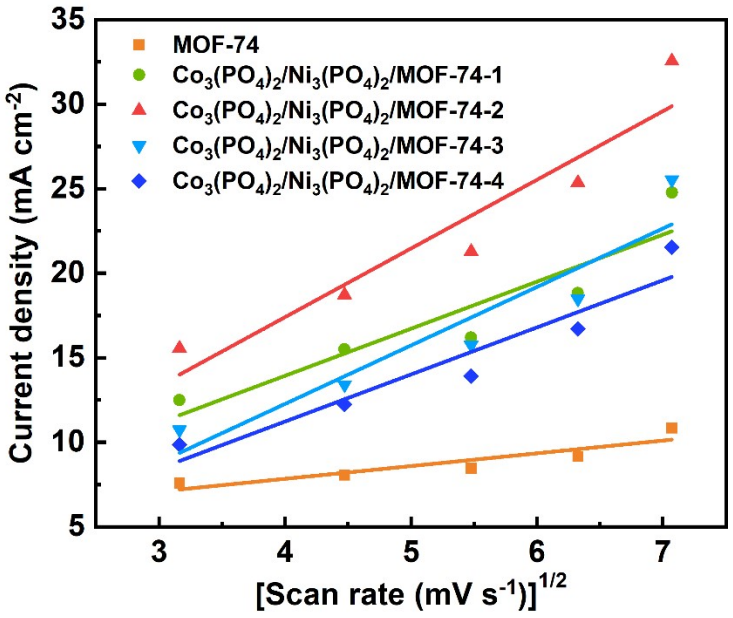

Fig. S10. The linear relationship between current densities and the square root of scan rates in 0.1 M KOH + 1.0 M CH_3CH_2OH for MOF-74, $Co_3(PO_4)_2$, and $Co_3(PO_4)_2/Ni_3(PO_4)_2$/MOF-74-*x* (*x* = 1, 2, 3, 4) heterojunctions.

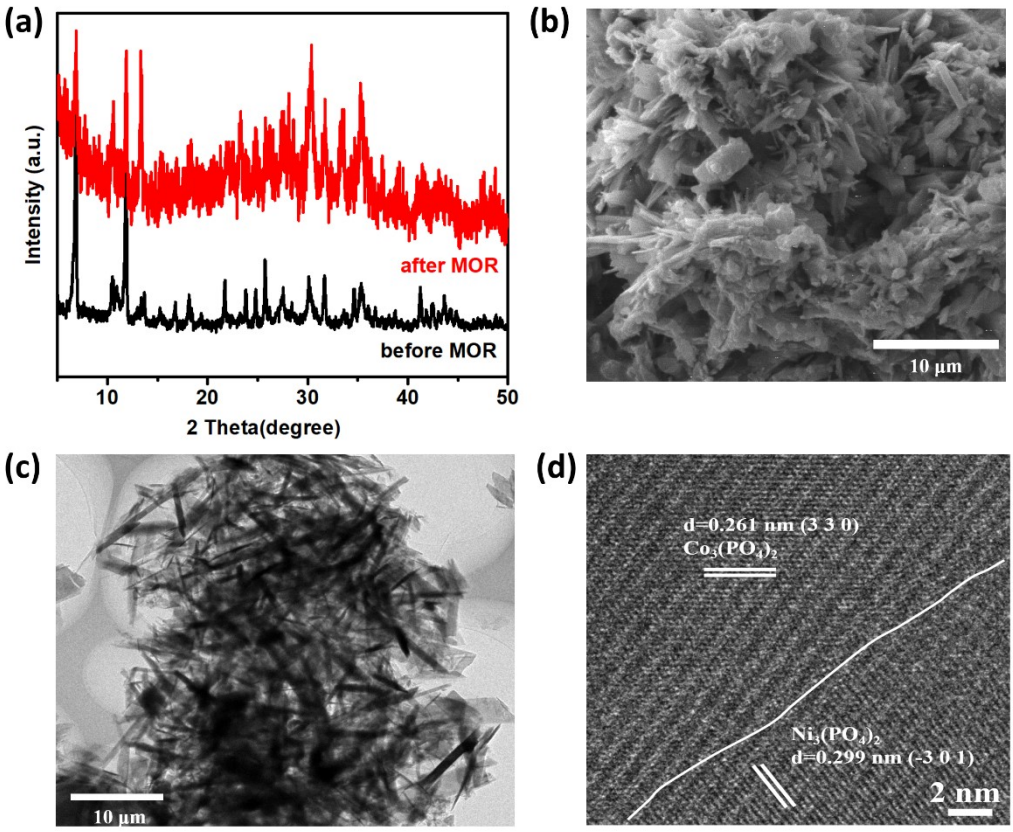

Fig. S11. (a) PXRD pattern, (b) SEM image, and (c)/(d) TEM images of the $Co_3(PO_4)_2/Ni_3(PO_4)_2$/MOF-74-2 after electrocatalysis (MOR).

Table S1. The comparison of the MOR properties between $Co_3(PO_4)_2/Ni_3(PO_4)_2$/MOF-74-2 and some other reported catalysts.

Electrocatalysts	Peak current density (mA cm^{-2})	Scan rate (mV s^{-1})	Experimental conditions	References
$Co_3(PO_4)_2/Ni_3(PO_4)_2$/ MOF-74-2	27.5	50	0.1 M KOH + 1.0 M CH_3OH	This Work
NiCu	21	10	0.1 M NaOH + 0.2M CH_3OH	[1]
2 wt%GO/Co-MOF	17.6	50	1 M KOH+3 M CH_3OH	[2]

5 wt%GO/Co-MOF	29.1	50	1 M KOH + 3 M CH_3OH	[2]
Pt_1Ni_1/C	12	50	1 M KOH + 1 M CH_3OH	[3]
Ni-BTC/rGO	27.1	50	1.0 M KOH + 3.0 M CH_3OH	[4]
20% Ni/MIL-110	14.4	50	0.1 M NaOH + 1 M CH_3OH	[5]
Ni-BTC	27.2	50	1.0 M KOH + 2.0 M CH_3OH	[6]
$Ni_{100}Bi_1$	35.1	50	1 M NaOH + 1M CH_3OH	[7]
NiO-Ni-P	28.6	50	0.5 M KOH + 1 M CH_3OH	[8]
Ni nanoflower	21.3	50	0.5 M KOH + 1 M CH_3OH	[6]
$NiMoO_4$	49	50	1 M KOH + 2 M CH_3OH	[9]
Ni-Ni-2	24.6	50	0.1 M KOH + 1.0 M CH_3OH	[8]
NiPx-R	100 (1.49 V)	0.05	1 M KOH + 0.5 M CH_3OH	[10]
20% Ni-N-C	~610 mA mg^{-1}	50	1 M KOH + 1 M CH_3OH	[11]
NiCo-MOF-P	170	50	1 M KOH + 0.5 M CH_3OH	[12]
Cu/NiMOF@5 wt% g-C_3N_4	103.42	50	1 M NaOH + 3 M CH_3OH	[13]
MOF-74(Ni)/NiOOH	27.62	50	0.1 M KOH + 1 M CH_3OH	[14]
Ni-BTC/NiS_2	34.36	50	0.1 M KOH + 1 M CH_3OH	[15]
CuO-C/$NiCo_2O_4$	194.6	50	1 M NaOH + 1 M CH_3OH	[16]
Ni/NiO/RG	79.5	50	1 M KOH + 1 M CH_3OH	[17]
Ni-MOF nanorods	~18	10	0.1 M NaOH + 0.2 M CH_3OH	[18]
rGO@Mn-Co/C	235.24	50	1 M NaOH + 3 M CH_3OH	[19]
a-NiCo-MOFNWs-P	216.8 (0.6 V)	50	1 M KOH + 1 M CH_3OH	[20]

References

1. R. M. Ding, J. P. Liu, J. Jiang, F. Wu, J. H. Zhu, X. T. Huang, Tailored Ni-Cu alloy hierarchical porous nanowire as a potential efficient catalyst for DMFCs, *Catal. Sci. Technol*., 2011, **1**, 1406.
2. R. Mehek, N. Iqbal, T. Noor, H. Nasir, Y. Mehmood, S. Ahmed, Novel Co-MOF/Graphene Oxide Electrocatalyst for Methanol Oxidation, *Electrochim. Acta*, 2017, **255**, 195.
3. S. Q. Lu, H. M. Li, J. Y. Sun, Z. B. Zhuang, Promoting the methanol oxidation catalytic activity by introducing surface nickel on platinum nanoparticles, *Nano Res*., 2018, **11**, 2058.
4. L. Yaqoob, T. Noor, N. Iqbal, H. Nasir, N. Zaman, Development of Nickel-BTC-MOF-Derived Nanocomposites with rGO Towards Electrocatalytic Oxidation of Methanol and Its Product Analysis, *Catalysts*, 2019, **9**, 856.
5. Y. Wang, C. Liu, J. Xiang, L. Xing, X. Ou, S. Chen, X. Xue, F. Yu, R. Li, Electrocatalytic oxidation of methanol on nickel doped metal-organic frameworks MIL-110 modified glassy carbon electrode in alkaline medium, *Int. J. Electrochem. Sci*., 2019, **14**, 5247.
6. J.-Y. Luo, F.-C. Hu, B.-J. Xi, Q.-W. Han, X.-Q. Wu, Y.-P. Wu, Q. Zhang, R. Chi, D.-S. Li, *Inorg. Chem. Commun*., 2022, **143**, 109777.
7. P. Gao, Y. Gu, P. Li, Z. Yu, Y. Hu, C. Zhang, Z. Xu, Y. An, Promoting effect of Bi in Ni-Bi oxide electrocatalysts for methanol oxidation reaction, *J. Mater. Sci. Mater. Electron*., 2020, **31**, 13219.
8. S. Liu, Y.-Y. Sun, Y.-P. Wu, Y.-J. Wang, Q. Pi, S. Li, Y.-S. Li, D.-S. Li, Common strategy: Mounting the rod-like Ni-based MOF on hydrangea-shaped nickel hydroxide for superior electrocatalytic methanol oxidation reaction, *ACS Appl. Mater. Interfaces*, 2021, **13**, 26472.
9. P. R. Jothi, S. Kannan, G. Velayutham, Enhanced methanol electro-oxidation over in-situ carbon and graphene supported one dimensional $NiMoO_4$ nanorods, *J. Power Sources*, 2015, **277**, 350.

10. S. Li, R. Ma, J. Hu, Z. Li, L. Liu, X. Wang, Y. Lu, G. E. Sterbinsky, S. Liu, L. Zheng, J. Liu, D. Liu, J. Wang, Coordination environment tuning of nickel sites by oxyanions to optimize methanol electro-oxidation activity, *Nat. Commun.*, 2022, **13**, 2916.
11. Z. Zhou, J. Zhang, S. Mukherjee, S. Houd, R. Khare, M. Dblinger, O. Tomanec, M. Otyepka, M. Koch, P. Gao, L. Zhou, W. Li, R. A. Fischer, Porphyrinic MOF derived Single-atom electrocatalyst enables methanol oxidation, *Chem. Eng. J.*, 2022, **449**, 137888.
12. M. M. Rajpure, H. S. Jadhav, H. Kim, Advanced LDH-MOF derived bimetallic NiCoP electrocatalyst for methanol oxidation reaction, *Col. Ioid. Surface A.*, 2022, **654**, 130062.
13. M. Abbasil, T. Noor, N. Iqbal, N. Zaman, Electrocatalytic study of cu/Ni MOF and its g-C_3N_4 composites for methanol oxidation reaction, *Int. J. Energy Res.*, 2022, **46**, 13915.
14. W.-Q. Zhou, B.-J. Xi, X.-W. Chang, B. Wang, X.-Q. Wu, S. Li, Y.-P. Wu, D.-S. Li, Facile In Situ Transformation of NiOOH into MOF-74(Ni)/NiOOH Heterogeneous Composite for Enchancing Electrocatalytic Methanol Oxidation, *Molecules*, 2022, **27**, 2113.
15. J.-Y. Luo, F.-C. Hu, B.-J. Xi, Q.-W. Han, X.-Q. Wu, Y.-P. Wu, Q. Zhang, R. Chi, D.-S. Li, Fabricating of Ni-BTC/NiS_2 heterostructure via self-assembly strategy for electrocatalytic methanol oxidation, *Inorg. Chem. Commun.*, 2022, **143**, 109777.
16. S. Sheikhi, F. Jalali, Hierarchical $NiCo_2O_4$/CuO-C nanocomposite derived from copper-based metal-organic framework and Ni/Co hydroxides: Excellent electrocatalytic activity towards methanol oxidation, *J. Alloy Compd.*, 2022, **907**, 164510.
17. K. Zhang, Y. Han, J. Qiu, X. Ding, Y. Deng, Y. Wu, G. Zhang, L. Yan, Interface engineering of Ni/NiO heterostructures with abundant catalytic active sites for enhanced methanol oxidation electrocatalysis, *J. Colloid. Interf. Sci.*, 2023, **630**, 570.
18. S. Radhakrishnan, S. C. Selvaraj, T. H. Ko, J. Mathiyarasu, B.-S. Kim,

Environmental-assisted simple synthesis and electrocatalytic performance of Ni-MOF nanorods, *Electrochim. Acta*, 2023, **462**, 142798.

19. N. Zaman, N. Iqbal, T. Noor, Comparative study of Mn-ZIF-67 derived carbon (Mn-Co/C) and its rGO-based composites for the methanol oxidation, *J. Environ. Chem. Eng*., 2022, **10**, 108351.
20. M. Han, Z. Zhao, X. Zhang, P. Wang, L. Xing, D. Jia, L. Wang, X. Chen, H. Gao, G. Wang, Phosphorus-Doped directly interconnected networks of amorphous Metal-Organic framework nanowires for efficient methanol oxidation, *J. Colloid Interf. Sci*., 2023, **641**, 675.